Rev. Roum. Sci. Techn.– Électrotechn. et Énerg.
Vol. **67**, *3*, pp. 287–292, Bucarest, 2022

HARDWARE IN THE LOOP EXPERIMENTAL ASSESSMENT OF PERTURB AND OBSERVE AND IC STATEFLOW PHOTOVOLTAIC MAXIMUM POWER POINT TRACKING SYSTEM

ABDELGHANI HARRAG[1], MUSTAPHA HATTI[2]

Keywords: Photovoltaic; Maximum power point tracking; Perturb and observe; Incremental conductance; Stateflow; STM32F4.

This paper deals with the development of the stateflow perturb and observe (P&O) and incremental conductance (IC) maximum power point tracking (MPPT) controllers. The photovoltaic (PV) power system is composed of PV module BP-SX150S powering a resistive load via a dc-dc boost converter controlled using the proposed stateflow models. The proposed stateflow MPPT controllers have been tested and validated in simulation and experimental mode using different test scenarios, including PV characteristics, variation in insolation, variation in temperature, and variation in duty cycle step. Simulation results show that both proposed stateflow P&O and IC MPPT models effectively track the maximum output power regarding all considered scenarios tests with the best performance for the variable step size versions. Experimental results obtained using the STM32F4 board in the processor in the loop mode confirm the simulation results.

1. INTRODUCTION

During the last decades, distributed generation (DG) systems based on renewable energy sources, such as wind turbines, fuel cells, and photovoltaics, have been proposed to overcome the challenges of integrating renewable energy sources into the existing microgrid. Dc/ac power electronics converter has been widely used to interface the DGs-based renewable energy sources and energy storage system. The penetration of power electronic converters into the existing utility grid has increased at the same time as renewable energy, Consequently, the rotating inertia of the power system is reduced, which could cause a stability problem. In recent years, many researchers have focused on developing inverter-based DG control strategies to facilitate the integration of renewable energy into the main grid [1–4].

Due to environmental climate change impacts and global warming problems caused by the large consumption of fossil fuels, we cannot continue the same energy model based mainly on the consumption of finite energy resources indefinitely. In this context, in the last decade, we have observed the emergence of a new energy model based on renewable energies, the reason for this transition is simple and imperative: there is no other way, no alternative [1]. Because of environmental and climate alarms, as well as awareness and government support, boosted by the drop in systems costs and the increase in energy demand, the transition to the green energy model is growing rapidly. Among renewable energies, PV is the second-most deployed renewable technology in terms of global installed capacity, after wind with 44 %, 33 %, and 18 %, respectively. The PV capacity is expected to reach 970 GW in 2025 [2–3].

Apart from the problem of module performance on which research continues, and the price that can be considered as a solved problem this last decade, the PV offers enormous advantages among them: i) PV fuel is free; ii) PV produces no noise, harmful emissions or polluting gases which contributes in reducing global warming; iii) PV modules lifetime is about 30 years showing their safety and high reliability; iv) PV modules require virtually no maintenance and can be recycled; v) PV will be a key component of future positive energy buildings; and vi) PV is able to bring electricity to remote rural areas [5]**.**

Conversely, the PV systems suffer from the energy source irregularity and nonlinearity of output characteristics which vary heavily with atmospheric conditions such as temperature and irradiance. As a results, the PV systems need the use of power conversion stage to adapt the transfer of the available power to the load via the use of maximum power point tracking controller [6–8].

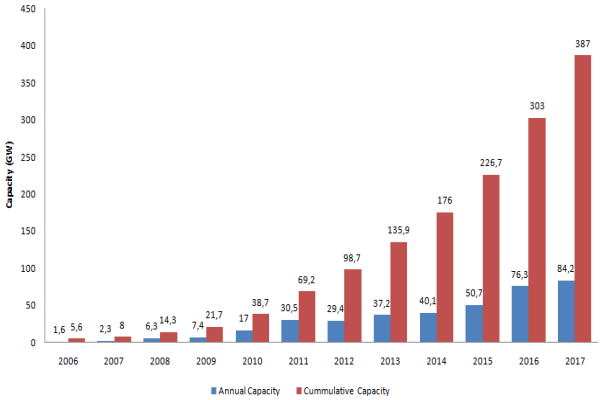

Fig. 1 – World's PV installed capacity.

Accordingly, the last two decades have seen the development of several MPPT controllers. Most of them use the classical perturb and observation based [9, 10], hill climbing [11], and incremental conductance [12, 13] algorithms. Other authors propose controllers based on the fraction of short circuit current [14] or open circuit voltage [15]. Soon many researchers propose intelligent MPPT controllers based on fuzzy logic [16], artificial neural networks [17, 18], genetic algorithms [19], particle swarm optimization [20], and ant colony optimization [21] methods.

In this work, we propose the hardware-in-the-loop (HIL) assessment of the P&O and IC PV MPPT controllers developed previously using stateflow models [22]. The proposed models have been implemented and validated

[1]Mechatronics Laboratory, Electrical Engineering Department, Faculty of Technology, Ferhat Abbas University Setif 1, Setif 19000, Algeria, E-mail: a.harrag@univ-setif.dz
[2]UDES, Unité de Développement des Equipements Solaires, EPST-CDER, Bou Ismail, BP386, 42415, Tipasa, Algeria, E-mail : m.hatti@ieee.org

using a PV system composed of PV module BP-SX150S powering a resistive load via a dc-dc boost converter controlled using the proposed stateflow models. Simulation results obtained under different test scenarios, including variable insolation, temperature, and duty cycle step, show that both proposed stateflow P&O and IC MPPT models effectively track the maximum output power regarding all considered scenarios tests. In addition, experimental results obtained using the STM32F4 board in the processor in the loop mode confirm the good tracking capability of both developed Stateflow models.

The rest of this paper is organized as follows: section 2 gives the material and methods used in this study, including the PV cell modeling, the classical as well as the proposed stateflow MPPT controllers' description. Section 3 presents the results and discussions, while section 4 states the main conclusions of this work.

2. **MATERIAL AND METHODS**

2.1. PV CELL MODELLING

A model that is widely used and based on the well-known Shockley diode equation is presented below in Fig. 2 [23].

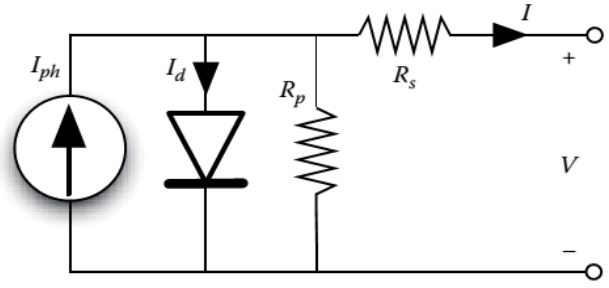

Fig. 2 – Solar cell single-diode model.

The output current I can be expressed by:

$$I = N_p I_{ph} - N_p I_{rs}\left[\mathrm{e}^{\left(\frac{q(V+R_eI)}{A.k.T.N_s}\right)} - 1\right] - N_p\left(\frac{q(V+R_eI)}{N_sR_p}\right), \quad (1)$$

where: V is the cell output voltage; q is the electron charge (1.60217646×10^{-19} C); k is the Boltzmann's constant (1.3806503×10^{-23} J/K); T is the temperature in Kelvin; I_{rs} is the cell reverse saturation current; A is the diode ideality constant; N_p and N_s are the numbers of PV cells connected parallel and in series, respectively.

The generated photocurrent I_{ph} is related to the solar irradiation by the following equation:

$$I_{ph} = \left[I_{sc} + k_i\left(T - T_r\right)\right]\frac{S}{1000}, \quad (2)$$

where: k_i is the short-circuit current temperature coefficient; s is the solar irradiation in W/m^2; T_r is the cell reference temperature; I_{sc} is the cell short-circuit current at a reference temperature.

The cell's saturation current varies with temperature according to the following equation:

$$I_{rs} = I_{rr}\left(\frac{T}{T_r}\right)^3 \exp\left(\frac{q.E_G}{A.k}\left(\frac{1}{T_r} - \frac{1}{T}\right)\right), \quad (3)$$

where E_g is the band-gap energy of the semiconductor and I_{rr} is the reverse saturation at T_r.

2.2. PV MPPT

The maximum power point tracker plays a considerable role in the performance improvement of the PV system. Among cited MPPT algorithms and considering simplicity and easiness of implementation, the P&O and the IC MPPTs are the most used [23].

2.2.1. P&O MPPT

According to the P–V characteristics, the maximum power point corresponds to the point given by ($\mathrm{d}P/\mathrm{d}V = 0$). To reach this point, the perturb and observe MPPT algorithm seeks the maximum power point through the voltage perturbation based on the results of the comparison of the output power ($\mathrm{d}P$) as well as the voltage ($\mathrm{d}V$) acquired during two successive samples (k) and (k – 1). If $\mathrm{d}P$ is positive, the voltage is increased if $\mathrm{d}V$ is positive, otherwise, the voltage is decreased. If $\mathrm{d}P$ is negative, the voltage is increased if $\mathrm{d}V$ is negative, otherwise, the voltage is increased [24].

2.2.2. IC MPPT

The incremental conductance algorithm uses each time the acquired – current and voltage to compute the conductance and the incremental conductance based on the following equations [25]:

$$\frac{\mathrm{d}P}{\mathrm{d}V} = \frac{\mathrm{d}(I.V)}{\mathrm{d}V} = I + V\frac{\mathrm{d}I}{\mathrm{d}V} = 0, \quad (4)$$

$$\frac{\mathrm{d}I}{\mathrm{d}V} = -\frac{I}{V} \text{ at } MPP, , \quad (5)$$

$$\frac{\mathrm{d}I}{\mathrm{d}V} > -\frac{I}{V} \text{ at the left of } MPP, , \quad (6)$$

$$\frac{\mathrm{d}I}{\mathrm{d}V} < -\frac{I}{V} \text{ at the right of } MPP, \quad (7)$$

.

2.3. PROPOSED STATEFLOW MPPT MODELS

Stateflow allows us to simulate the behavior of hybrid systems of discrete and continuous events. It models the behavior of systems that move from one state to another (called state machine with a finite number of states) in response to actions (called discrete events). Stateflow model allows to draw of state and flow charts in the same model. It provides seamless integration of state machines into a block diagram formalism. Figures 3 and 4 show the implemented P&O and the IC MPPTs stateflow models.

3. **RESULTS AND DISCUSSION**

3.1. SIMULATION TESTS

The proposed stateflow MPPT controllers have been investigated using Matlab/Simulink PV system model. This later includes a BP-SX150S fed by the implemented stateflow MPPTs driving the boost dc-dc converter and powering a resistive load, as shown in Fig. 3.

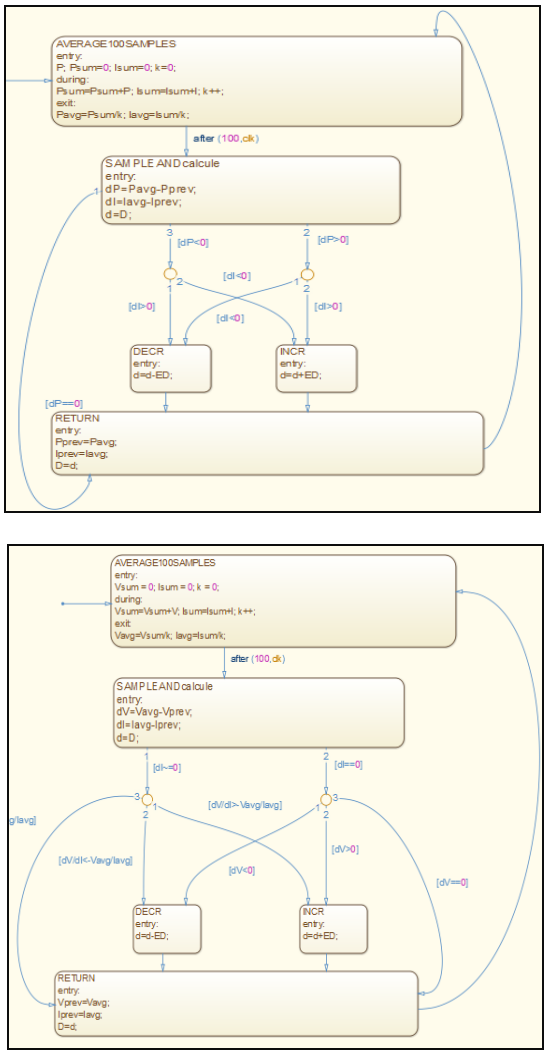

Fig. 3 – Implemented Stateflow MPPTs: P&O (above) and IC (below).

Table 1 gives the BP-SX150S electrical characteristics, while Table 2 summarizes the dc-dc boost converter parameters.

Table 1

Electrical Characteristics of BP-SX150S (1 kW/m², 25 °C)

Description	BP-SX150S
Maximum Power (P_{MPP}) [W]	150
Voltage P_{max} (V_{MPP}) [V]	34.5
Current at P_{max} (I_{MPP}) [A]	4.35
Short Circuit current (I_{sc}) [A]	4.75
Open Circuit voltage (V_{oc}) [V]	43.5
Temperature coeff. of V_{oc} [mV/°C]	-0.38
Temperature coeff. of I_{sc} [% °C]	0.065
Temperature coeff. of power [% °C]	-0.50
NOCT (°C)	47

Table 2

Boost dc-dc converter parameters

Parameters	Value
L (µH)	220
C_1 (µF)	95
C_2 (µF)	217.5
R_L (Ω)	20
F_S (kHz)	50

The evaluation of the proposed stateflow MPPT models has been carried out using MATLAB / Simulink environment considering different test scenarios: Test scenario 1: *P–V* characteristics, Test scenario 2: Irradiation change, Test scenario 3: Temperature change, and Test scenario 4: Step Size change.

3.1.1. Test scenario 1 – *P–V* characteristics

This test scenario permits validating the PV characteristics (*P–V* and *I–V*) generated by both implemented P&O and IC stateflow MPPTs. Figure 4. shows the obtained PV characteristics using P&O and IC stateflow MPPT models, respectively.

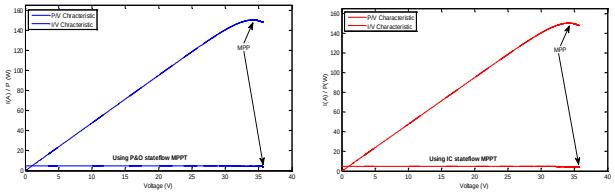

Fig. 4 – *P–V* and *I–V* characteristics using stateflow MPPTs: P&O (left) and IC (right).

From Fig. 4, we can notice that the proposed stateflow MPPT models reproduce the *P–V* characteristics with good fidelity.

3.1.2. Test scenario 2 – irradiation change

In this scenario, we use an irradiation change defined as follows: 600 W/m² from 0 s to 3 s, 800 W/m² from 3 s to 6 s, and 1000 W/m² from 6s to 9 s. Figure 5 shows the output power variation under irradiation change using the proposed stateflow P&O and IC MPPTs, respectively.

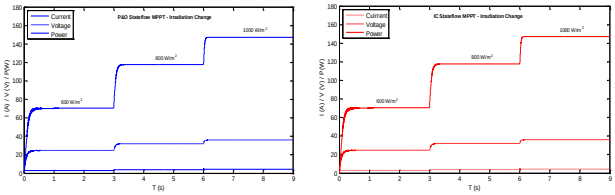

Fig. 5 – *P–V* output power, voltage and current under variant irradiation conditions using stateflow MPPTs: P&O (left) and IC (right).

From Fig. 5, we can see that stateflow MPPT models effectively track the maximum output power. The maximum output power corresponds to the expected theoretical value of 90 W for 600 W/m², 120 W for 800 W/m², and 150 W for 1000 W/m², respectively.

3.1.3. Test scenario 3 – temperature change

For this scenario, we use a temperature change: 25 °C from 0 s to 3 s, 50 °C from 3 s to 6 s and 75 °C from 6 s to 9 s. Figure 6 shows the output power variation under temperature change using the proposed stateflow P&O and IC MPPTs, respectively.

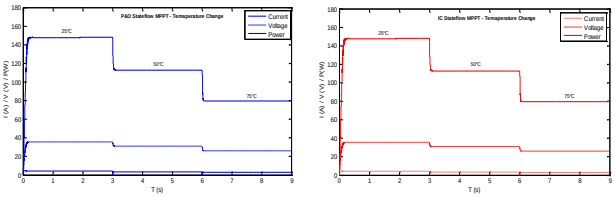

Fig. 6 – *P–V* output power, voltage and current under variant temperature using stateflow MPPTS: P&O (left) and IC (right).

3.1.4. Test scenario 4 – step size change

In this scenario, we evaluate the proposed stateflow models considering the two developed versions (fixed step size and variable step size). Firstly, the fixed step size was evaluated using 0.001 s, 0.005 s, and 0.1 s as step sizes. Secondly, the fixed step size version has been compared to the variable step size one, which uses a step size equal to 0.001 s scaled by a

scaling factor between 0.1 and 10 which corresponds to a variation of the step size between 0.0001 s (close to the MPP) and 0.01 s (far from the MPP). Figure 7 shows the output power using the fixed step size state flow MPPTs.

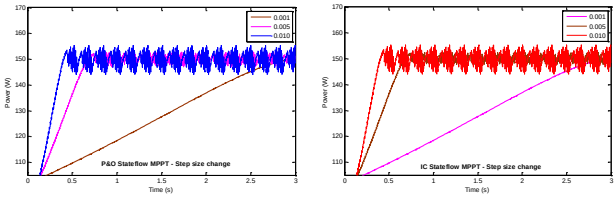

Fig. 7 – Output power under varying step size using stateflow MPPTs: P&O (left) and IC (right).

In Fig. 7, the proposed stateflow models track the maximum output power using the corresponding step size value. We can see the effect of the step size on the maximum output power profile with fewer oscillations and long response time with a small step size and more oscillations and fast response time with a large step size.

To evaluate the developed two versions of the stateflow MPPTs (fixed and variable step size versions), we consider the response time for the dynamic performance and the oscillations around the MPP point for the static performances. Figure 8 shows the dynamic performance of both fixed and variable step size stateflow MPPTs for both algorithms.

In Fig. 8, we can see that the proposed variable stateflow MPPTs rapidly track the maximum output power compared to the fixed step-size ones. The variable step size response time is around 1/3 (~0.3 s for the variable version instead of 0.75 s for the fixed step size version).

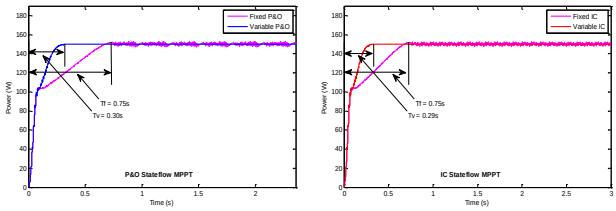

Fig. 8 – Response time of output power using stateflow MPPTs: P&O (left) and IC (right).

Figure 9 shows the static performance of both fixed and variable step size stateflow MPPTs for both algorithms.

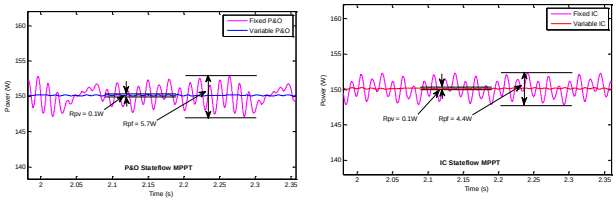

Fig. 9 – Output power oscillations using stateflow MPPTs: P&O (left) and IC (right).

In Fig. 9, the proposed variable stateflow MPPTs outperform the fixed step size version regarding the static performance. The variable step size oscillation is around 0.1 W for both algorithms, while the corresponding fixed step size oscillation is between 4.4 W for the IC MPPT and 5.7 W for the P&O MPPT. From different scenarios tested and obtained results, the main contributions of this work are: i) the stateflow implementation of P&O as well as IC MPPTs; ii) comparative study between the fixed step size and variable step size implemented stateflow MPPT versions, to our knowledge, and unless we are mistaken, the variable step size MPPT P&O and IC stateflow implementations are a pioneering work; and iii) the ability of the proposed stateflow MPPTs to track effectively the maximum power point with good accuracy and performances in static and dynamic states considering different scenario tests including insolation, temperature and step size variation.

3.2. EXPERIMENTAL TESTS

In this part, we use a HIL testing technique where real signals from a controller are connected to a test system that simulates reality, tricking the controller into thinking it is in the assembled product. Test and design iteration takes place as though the real-world system is being used. The experimental validation of the proposed stateflow MPPTs has been carried out using the STM32F4 Discovery board via the hardware in the loop mode. Figure 10 presents the illustrated and real hardware in the loop process using the STM32F4 Discovery board. The inputs are the current and voltage; the output is the PWM ratio computed using the generated and transferred code of the proposed stateflow MPPTs.

The STM32F4 Discovery offers the following features:

- STM32F407VGT6 microcontroller featuring 32-bit Arm®(a) Cortex®-M4 with FPU core, 1-Mbyte Flash memory, 192-Kbyte RAM in an LQFP100 package;
- USB OTG FS;
- ST MEMS 3-axis accelerometer;
- User and reset push-buttons;
- Eight LEDs;
- Board connectors;
- Flexible power-supply options: ST-LINK, USB VBUS, or external sources;
- External application power supply: 3 V and 5 V;
- Comprehensive free software including a variety of examples, part of STM32CubeF4 MCU Package, or STSW-STM32068 for using legacy standard libraries;
- On-board ST-LINK/V2-A debugger/programmer with USB re-enumeration capability: mass storage, Virtual COM port, and debug port.

To assess experimentally the proposed stateflow P&O and IC MPPTs, the implemented controllers have been validated considering the same test scenarios used in the simulation tests: Test scenario 1: *P–V* characteristics, Test scenario 2: Irradiation change, Test scenario 3: Temperature change and Test scenario 4: Step size change.

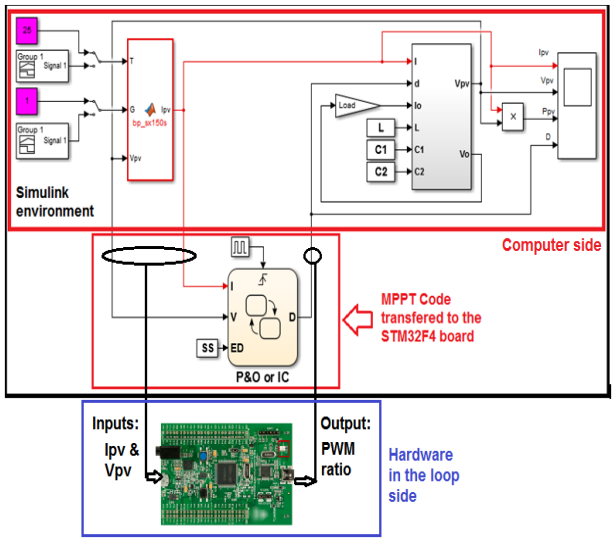

Fig. 10 – Hardware in the loop experimental mode.

3.2.1. Test scenario 1 – *P–V* characteristics

As in simulation tests, this test scenario permits the experimental validation of the PV characteristics (P-V) generated by both implemented P&O and IC stateflow MPPTs. Figure 11 shows the obtained PV characteristics using P&O and IC stateflow MPPT models.

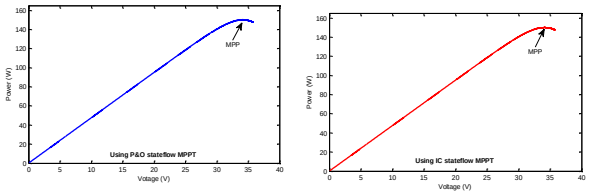

Fig. 11 – *P–V* characteristic using HIL stateflow MPPTs: P&O (left) and IC (right).

3.2.2. Test scenario 2 – irradiation change

In this scenario, we use the same irradiation change used in simulation tests: 600 W/m^2 from 0s to 3 s, 800W/m^2 from 3 s to 6 s and 1000 W/m^2 from 6 s to 9 s.

Figure 12 shows the output power variation under irradiation change using the proposed stateflow P&O and IC MPPTs, respectively. In Fig. 12, as noticed in simulation tests, we can see that proposed stateflow MPPTs effectively track the maximum output power in case of irradiation change.

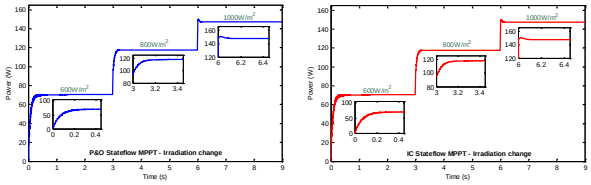

Fig. 12 – The output power variation using under different irradiation changes using stateflow MPPTs: P&O (left) and IC (right).

3.2.3. Test scenario 3 – temperature change

For this scenario, we use a temperature change: 25 °C from 0 s to 3 s, 50 °C from 3 s to 6 s, and 75 °C from 6 s to 9 s. Figure 13 shows the output power variation under temperature change using the proposed stateflow P&O and IC MPPTs.

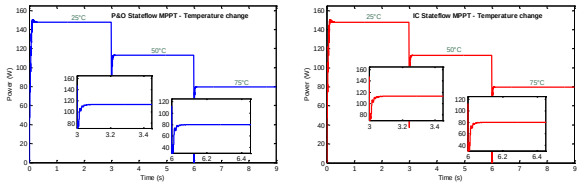

Fig. 13 – The output power variation using under varying temperature using stateflow MPPTs: P&O (left) and IC (right).

3.2.4 Test scenario 4 – step size change

In this scenario, we evaluate the proposed stateflow models using different step sizes: 0.001 s, 0.005 s, and 0.1 s. Figuire 14 shows the output power using the fixed step size state flow P&O and IC MPPTs.

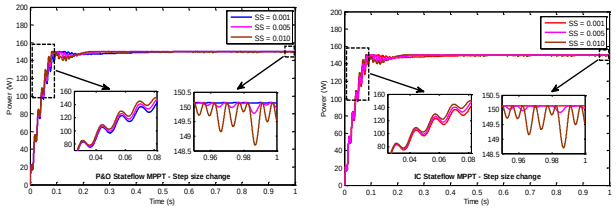

Fig. 14 – Output power using fixed step size stateflow P&O MPPT under varying step size.

In Fig. 14, the proposed stateflow models track the maximum output power using the corresponding step size value. As noticed for the simulation tests, we can see the effect of the step size on the maximum output power profile with fewer oscillations and long response time with a small step size (blue line for the P&O and red line for the IC and more oscillations and fast response time with large step size (brown line for P&O as well as for IC).

4. CONCLUSIONS

The assessment of the two well-known perturb and observation and the incremental conductance maximum power point tracking algorithms have been investigated using the implemented stateflow controller models under Matlab / Simulink environment. The simulation obtained results using a photovoltaic system composed of a BP-SX150S photovoltaic module fed by the implemented stateflow models controlling a dc-dc boost converter powering a resistive load under different test scenarios, including photovoltaic characteristics, irradiation change, temperature change, and step size change prove that the proposed models can effectively track the maximum power in all considered test cases. In addition, a comparative study between the proposed fixed step size stateflow models and the variable step size models has been carried out, showing that the varying step size versions outperform the fixed step size one. Experimental results obtained using the STM32F4 board in the hardware in the loop mode validate the simulation results.

ACKNOWLEDGMENTS

The Algerian Ministry of Higher Education and Scientific Research via DGRSDT supported this research (Research PRFU Project code: A01L07UN190120180005).

Received on 19 January 2020

REFERENCES

1. European Renewable Energy Council (EREC), *Renewable Energy in Europe Markets, Trends and Technologies*, Earthscan, London, United Kingdom, 2010.
2. D. Rekioua, E. Matagne, *Optimization of Photovoltaic Power Systems: Modelization, Simulation and control*, Springer, London, 2012.
3. *IRENA_Roadmap* 2016, Retrieved 30.10.2018 from http://www.irena.org/DocumentDownloads/Publications/IRENA_REmap_2016_edition_report.pdf
4. Y. Daili, A. Harrag, *Improved decoupling virtual synchronous generator control strategy*, Rev. Roum. Sci. Techn. – Électrotechn. et Énerg., **66**, *3*, pp. 153–160 (2021).
5. M. Hatti, *Operation and maintenance methods in solar power plants*, In: M. Sanz-Bobi (Edit.) Use, Operation and Maintenance of Renewable Energy Systems. Green Energy and Technology. Springer, Cham, pp. 61–93 (2014).
6. K.S.S. Tey, S. Mekhilef, *Modified incremental conductance MPPT algorithm to mitigate inaccurate responses under fast-changing solar irradiance level*, Solar Energy, **101,** pp. 333–342 (2014).
7. G.N. Femia, G. Petrone, G. Spagnuolo, M. Vitelli, *Optimization of perturb and observe maximum power point tracking method*, IEEE Trans Power Electron, **20**, pp. 963–973 (2005).
8. D.P. Winston, B.P. Kumar, S.C. Christabel, A.J. Chamkha, R. Sathyamurthy, *Maximum power extraction in solar renewable power system – a bypass diode scanning approach*, Computers & Electrical Engineering, **70**, pp. 122–136 (2018).
9. T. Radjai, J.P. Gaubert, L. Rahmani, S. Mekhilef, *Experimental verification of P&O MPPT algorithm with direct control based on Fuzzy logic control using CUK converter*, Int. Trans. Electr. Energ. Syst, **25**, *12*, pp. 3492–3508 (2015).
10. W. Xiao, W.G. Dunford, *A modified adaptive hill climbing MPPT method for photovoltaic power systems*, Proc. 35th Annu. IEEE Power Electron. Spec. Conf, pp. 1957–1963 (2004).
11. A. Harrag, A. Titraoui, H. Bahri, *P&O or IC for PV pumping system: what MPPT algorithm to improve performances?* 6th International Conference on Systems and Control (ICSC), 2017, pp. 220–225.

12. A. Harrag, S. Messalti, *IC-based variable step size neuro-fuzzy MPPT improving PV system performances*, Energy Procedia, **157**, pp. 362–374 (2019).
13. H. Ahmed Sher, A. Faisal Murtaza, A. Noman, K.E. Addoweesh, *A new sensorless hybrid MPPT algorithm based on fractional short-circuit current measurement and P&O MPPT*, IEEE Transaction on Sustainable Energy, **6**, *4*, pp. 1426–1434 (2015).
14. M.A.S. Masoum, H. Dehbonei, E.F. Fuchs, *Theoretical and experimental analyses of photovoltaic systems with voltage and current-based maximum power-point tracking*, IEEE Trans. Energy Convers., **17**, *4*, pp. 514–522 (2002).
15. A. Harrag, S. Messalti, *New combined fuzzy-IC variable step size MPPT reducing steady-state oscillations*, in M. Hatti (Edit.), *Renewable Energy for Smart and Sustainable Cities Artificial Intelligence in Renewable Energetic Systems*, Springer, 2019, pp. 376–383.
16. H. Boumaaraf, A. Talha, O. Bouhali, *A three-phase NPC grid-connected inverter for photovoltaic applications using neural network MPPT*, Renewable and Sustainable Energy Reviews, **49,** pp. 1171–1179 (2015).
17. S. Messalti, A. Harrag, A. Loukriz, *A new variable step size neural networks MPPT controller: review, simulation and hardware implementation*, Renewable and Sustainable Energy Reviews, **68**, pp. 221–233 (2017).
18. S. Hadji, J.P. Gaubert, F. Krim, *Real-time genetic algorithms-based MPPT: study and comparison (theoretical and experimental) with conventional methods*, Energies, **11**, *2*, 17 pp. (2018).
19. R.B.A. Koad, A.F. Zobaa, A. El-Shahat, *A novel MPPT algorithm based on particle swarm optimization for photovoltaic systems*, IEEE Transactions on Sustainable Energy, **8**, *2*, pp. 468–476 (2017).
20. S. Titri, C. Larbes, K.Y. Toumi, K. Benatchba, *A new MPPT controller based on the ant colony optimization algorithm for photovoltaic systems under partial shading conditions*, Applied Soft Computing, **58**, pp. 465-479 (2017).
21. A. Harrag, S. Messalti, *Innovative stateflow models assessment of P&O and IC PV MPPTs*, in: M. Hatti, M. (Edit.) *Renewable Energy for Smart and Sustainable Cities*. (ICAIRES 2018). Lecture Notes in Networks and Systems, Cham, **62**, Springer, 2019.
22. J.W. Bishop, *Computer simulation of the effects of electrical mismatches in photovoltaic cell interconnection circuits*, Solar Cells, **25**, 1, pp. 73–89 (1988).
23. D. Verma, S. Nema, A.M. Shandilya, S.K. Dash, *Maximum power point tracking (MPPT) techniques: recapitulation in solar photovoltaic systems*, Renewable and Sustainable Energy Reviews, **54**, pp. 1018–1034 (2016).
24. S. Motahhir, A. El Hammoumi, A. El Ghzizal, *Photovoltaic system with quantitative comparative between an improved MPPT and existing INC and P&O methods under fast varying of solar irradiation*, Energy Reports, **4**, pp. 341–350 (2018).
25 K. Ishaque, Z. Salam, G. Lauss, *The performance of perturb and observe and incremental conductance maximum power point tracking method under dynamic weather conditions*, Applied Energy, **119**, pp. 228–236 (2014).